Emission and Absorption Tuning in TADF B,N-Doped Heptacenes: Toward Ideal-Blue Hyperfluorescent OLEDs

Kleitos Stavrou, Subeesh Madayanad Suresh, David Hall, Andrew Danos,* Nadzeya A. Kukhta, Alexandra M. Z. Slawin, Stuart Warriner, David Beljonne, Yoann Olivier, Andrew Monkman, and Eli Zysman-Colman*

Developing high-efficiency purely organic blue organic light-emitting diodes (OLEDs) that meet the stringent industry standards is a major current research challenge. Hyperfluorescent device approaches achieve in large measure the desired high performance by combining the advantages of a high-efficiency thermally activated delayed fluorescence (TADF) assistant dopant with a narrowband deep-blue multi-resonant TADF (MR-TADF) terminal emitter. However, this approach requires suitable spectral overlap to support Förster resonance energy transfer (FRET) between the two. Here, a color tuning of a recently reported MR-TADF B,N-heptacene core through control of the boron substituents is demonstrated. While there is little impact on the intrinsic TADF properties—as both singlet and triplet energies decrease in tandem—this approach improves the emission color coordinate as well as the spectral overlap for blue hyperfluorescence OLEDs (HF OLEDs). Crucially, the red-shifted and more intense absorption allows the new MR-TADF emitter to pair with a high-performance TADF assistant dopant and achieve maximum external quantum efficiency (EQE$_{max}$) of 15% at color coordinates of (0.15 and 0.10). The efficiency values recorded for the device at a practical luminance of 100 cd m^{-2} are among the highest reported for HF TADF OLEDs with CIE$_y$ ≤ 0.1.

1. Introduction

Organic light-emitting diode (OLED) display technology is evolving at a brisk rate, with high-end ultra-high definition (UHD) 4K and 8K OLED displays already in the market. These high-resolution displays must meet stringent emission color standards (BT.2020-2),[1] which are defined according to the Commission International de l'Éclairage (CIE) 1931 as (0.13, 0.05), (0.17, 0.80), and (0.71, 0.29) for blue, green, and red, respectively.[2] At present, this color requirement is met through the use of absorptive filters or microcavities to deliver saturated blue, green, and red emission.[3,4] Unfortunately, this approach necessarily results in a reduced efficiency of the devices as unwanted emission wavelengths are rejected. An alternative and attractive solution to the issue of color purity is to develop materials with intrinsically narrowband emission.

Commercial OLED displays currently use organic triplet-triplet annihilation

K. Stavrou, A. Danos, N. A. Kukhta,[+] A. Monkman
Department of Physics
Durham University
Durham DH1 3LE, UK
E-mail: andrew.danos@durham.ac.uk

S. M. Suresh, D. Hall, A. M. Z. Slawin, E. Zysman-Colman
Organic Semiconductor Centre
EaStCHEM School of Chemistry
University of St Andrews
St Andrews KY16 9ST, UK
E-mail: eli.zysman-colman@st-andrews.ac.uk

D. Hall, D. Beljonne, Y. Olivier
Laboratory for Chemistry of Novel Materials
University of Mons
Mons 7000, Belgium

S. Warriner
School of Chemistry
University of Leeds
Woodhouse Lane, Leeds LS2 9JT, UK

Y. Olivier
Laboratory for Computational Modeling of Functional Materials
Namur Institute of Structured Matter
Université de Namur
Rue de Bruxelles, 61, Namur 5000, Belgium

[+]Present Address: Materials Science and Engineering Department, University of Washington, Seattle WA 98195-2120, USA

**ADVANCED
SCIENCE NEWS**
www.advancedsciencenews.com

**ADVANCED
OPTICAL
MATERIALS**
www.advopticalmat.de

(TTA) emitters for blue pixels. By virtue of the operational exciton harvesting mechanism, the internal quantum efficiency of blue OLEDs is presently capped at 62.5%. Organic thermally activated delayed fluorescence (TADF) materials, by contrast, can harvest 100% of the electrically generated excitons to produce light and achieve higher device efficiencies.[5] Similarly, organometallic phosphorescent OLEDs can generate high-efficiency OLEDs, although with significant intrinsic limitations for blue-emitting device in terms of their stability. These limitations arise as photon energies approach metal-ligand bond dissociation energies, and as thermal population of metal-centered states (particularly for d_6 metal complexes) leads to severe non-radiative decay.

The TADF mechanism involves the thermal upconversion of non-emissive triplet excitons into singlets via reverse inter-system crossing (RISC). A small energy gap between T_1 and S_1 (ΔE_{ST}) is necessary to achieve TADF, and this is ensured when there is spatial separation of the frontier orbitals, which is normally achieved in a highly twisted donor–acceptor (D–A) architecture. However, D–A TADF emitters typically emit from charge transfer (CT) states where there is a large reorganization in the excited state that leads to broad (70–100 nm) emission.[6,7] These broad emission bands interact poorly with the aforementioned color purity filters, while also making it difficult to engineer deep-blue emitters[8–10] and suitably high-triplet hosts.[11]

In particular, these broad CT emission bands dictate that for an emitter to achieve deep-blue color coordinates, the high energy onset of the photoluminescence or electroluminescence spectrum must reside at significantly shorter wavelengths than the peak. As these short-wavelength onsets are taken to represent the S_1 energy, to ensure a small ΔE_{ST} and efficient RISC the T_1 energy (from phosphorescence onset) must also be very high, frequently approaching, or even exceeding 3 eV. Suitable host materials—requiring T_1 energies higher than any emissive dopants to prevent host-triplet quenching—are exceedingly rare, a situation only exacerbated by widespread overreporting of T_1 values for new hosts.[11] Such new host materials also frequently end up with low T_1 values due to the inclusion of charge-transporting groups such as benzonitrile or carbazole, leaving researchers with the unenviable choice between adequate charge-transport and adequate host triplet energy. These unfortunate circumstances explain the continued widespread use of high-T_1 and moderately electron transporting DPEPO for D–A TADF OLEDs, despite the known instability of this host material.[12]

Multiresonant TADF (MR-TADF) compounds are an alternative class of TADF materials that are typically based on p- and n-doped nanographene (Figure S1, Supporting Information).[13,14] Because of their rigid structure, these compounds show narrowband emission, typically with full width of half maxima (FWHM) of around 20–30 nm. Thus, MR-TADF emitters show potential to generate the required deep blue emission demanded by industry, and support the development of stable, efficient, and pure blue narrowband emitting organic materials that are expected to revolutionize OLED displays.[15] MR-TADF compounds show TADF due to the alternating pattern of electron density between the ground and excited states that leads to small ΔE_{ST}, combined with upper-triplet crossings from thermally populated T_n states back to the emissive S_1

state.[16–19] The excited states thus possess a distinct short-range charge transfer (SRCT) character,[14,20,21] and MR-TADF compounds are endowed with high singlet radiative decay (k_r) rates of around 10^7 s^{-1}.[5,20]

Despite these advantages, the RISC rates reported for MR-TADF materials typically lag ~100 times slower than those of leading D–A or D–A–D TADF materials.[14,22,23] This limitation frequently leads to inefficient triplet harvesting and low performance of the OLEDs at practical luminance. To circumvent this limitation, MR-TADFs have recently found a parallel application as terminal emitters in hyperfluorescent (HF) OLEDs. Indeed, truly ground-breaking device performances have been achieved when pairing a high-RISC D–A assistant dopant with narrowband MR-TADF terminal emitters.[24–26] This performance is in some cases supported by spontaneous alignment of the MR-TADF with the substrate, thus improving optical outcoupling of the device,[26] although the specific loss mechanisms that occur under electrical excitation, including charge trapping and Dexter transfer,[27] remain poorly understood.

High-performance HF OLEDs rely on efficient energy transfer between the D–A TADF assistant dopant that is responsible for exciton harvesting and the MR-TADF terminal emitter. Förster resonance energy transfer (FRET) is understood to be the main mechanism for this transfer, and FRET efficiency is proportional to the overlap between the emission spectrum of the D–A TADF assistant dopant and the absorption spectrum of the MR-TADF terminal emitter. As a result, the compatibility of many MR-TADF materials is severely limited by the low molar extinction coefficient of their lowest energy absorption bands—those that predominantly overlap with the emission spectrum of the D–A TADF assistant dopant. Expanding the FRET compatibility of a specific terminal emitter requires increasing the spectral overlap between the assistant dopant and terminal emitter. This in turn requires development of deeper-blue D–A TADF assistant dopants, but such emitters (and suitable hosts) remain persistently elusive—a circumstance that has stimulated the rapid development of the alternate hyperfluorescence approach.[28] Clearly then, synthetic control over both the emission and absorption spectra[23,29–31] of MR-TADF materials is crucial to enable and optimize their use in HF OLEDs with available D–A TADF cohosts. Expanding FRET compatibility to cyan or green D–A TADFs may also eventually circumvent the dilemma of blue D–A TADF host requirements.

We previously reported a linear B,N-doped ladder-type heptacene that emits at 390 nm (near UV) with an FWHM of 31 nm (240 meV) in THF solution.[32] The material displayed weak TADF due in part to the large ΔE_{ST} of 0.31 eV, along with significant TTA contribution reflected in the extended ms-timescale of the emission decay.[32] Due to the near UV emission and subsequent paucity of suitable OLED hosts, the investigated device performance was poor and there were no D–A TADFs identified as compatible assistant dopants for HF OLEDs.[33] In the present report, we show how the replacement of the hydroxyl groups for mesityl substituents in *α*-3BNMes (**Figure 1**) leads to the desired red-shifting of the emission toward an ideal-blue emission color coordinate, as well as a red-shifting of the absorption that supports HF compatibility with available D–A TADF assistant dopants. Together, these changes in optical
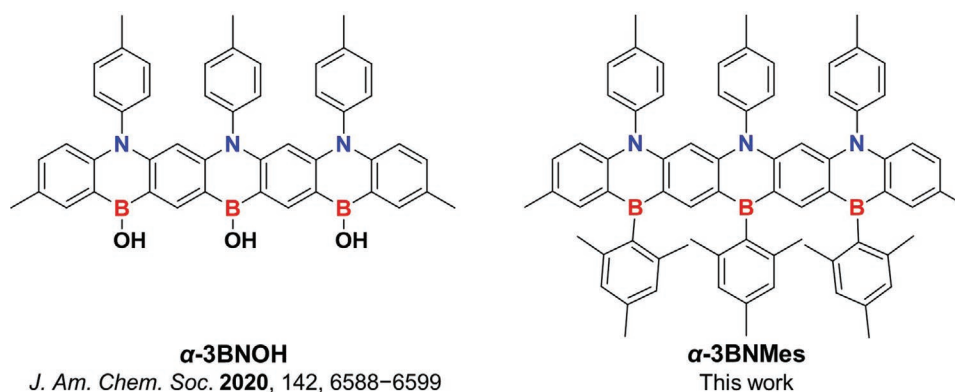
2200688 (2 of 9)

**ADVANCED
SCIENCE NEWS**

www.advancedsciencenews.com

**ADVANCED
OPTICAL
MATERIALS**

www.advopticalmat.de

α-3BNOH
J. Am. Chem. Soc. **2020**, 142, 6588−6599

α-3BNMes
This work

Figure 1. Structures of **α-3BNOH** and **α-3BNMes**.

properties compared to **α-3BNOH** allow **α-3BNMes** to be used in high-performance deep-blue HF OLEDs that show 15% maximum external quantum efficiencies (EQE_{max}) and color coordinates of (0.15 and 0.10). These results represent highly competitive device performance metrics at this color coordinate that are enabled by the finely-tuned emission and absorption spectra of **α-3BNMes** (Table S2, Supporting Information).

2. Results and Discussion

2.1. Synthesis

α-3BNMes was synthesized in three steps (Scheme S1, Supporting Information), where the key borylation step proceeds

in 57% yield. The identity and purity of **α-3BNMes** were established from a combination of ^{1}H NMR spectroscopy (**S2**), high-resolution mass spectrometry (**S4**), HPLC (**S5**), GPC trace analyses (**S7**), and single-crystal X-ray diffraction analysis (**Figure 2**). Like the parent compound (**α-3BNOH**), **α-3BNMes** shows high thermal stability, revealed by thermogravimetric analysis (TGA), with a decomposition temperature (T_d), defined as the 5% weight loss of the material, at 503 °C (Figure S8, Supporting Information).

We investigated the structure of **α-3BNMes** by growing single crystals via slow evaporation of the compound in THF. Full datasets were collected from many different crystals, and we report here our best result. The data obtained are adequate to demonstrate connectivity and gross structure but do not merit discussion of bond lengths (Figure 2). Like the parent
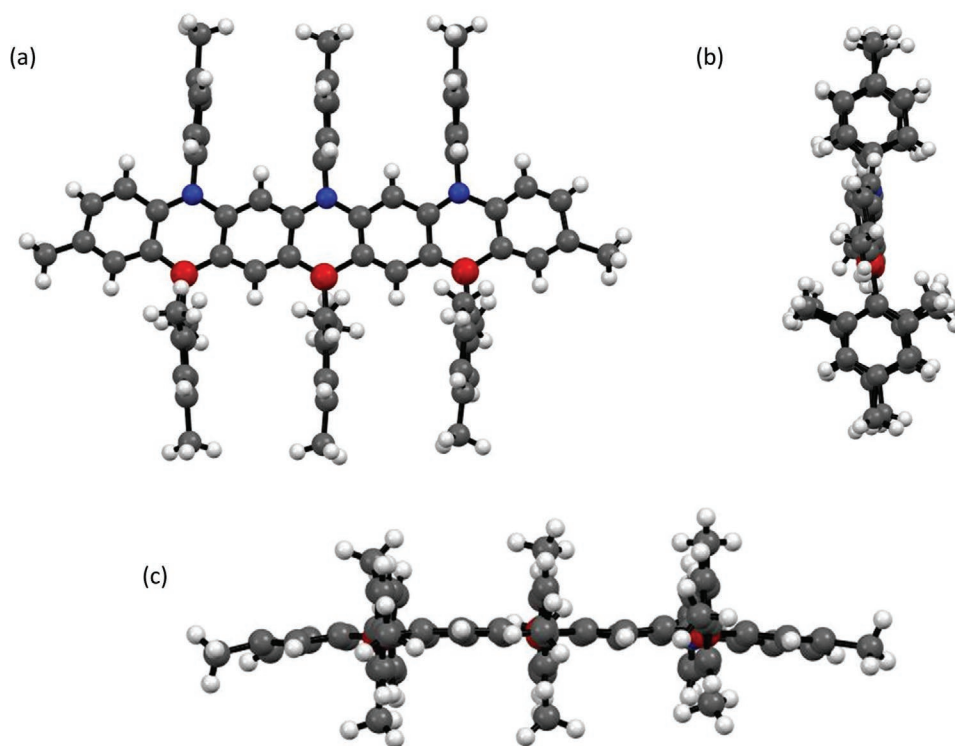

Figure 2. a) ball and stick representation of **α-3BNMes** obtained by single-crystal X-ray analysis. b) Side and c) plane views.
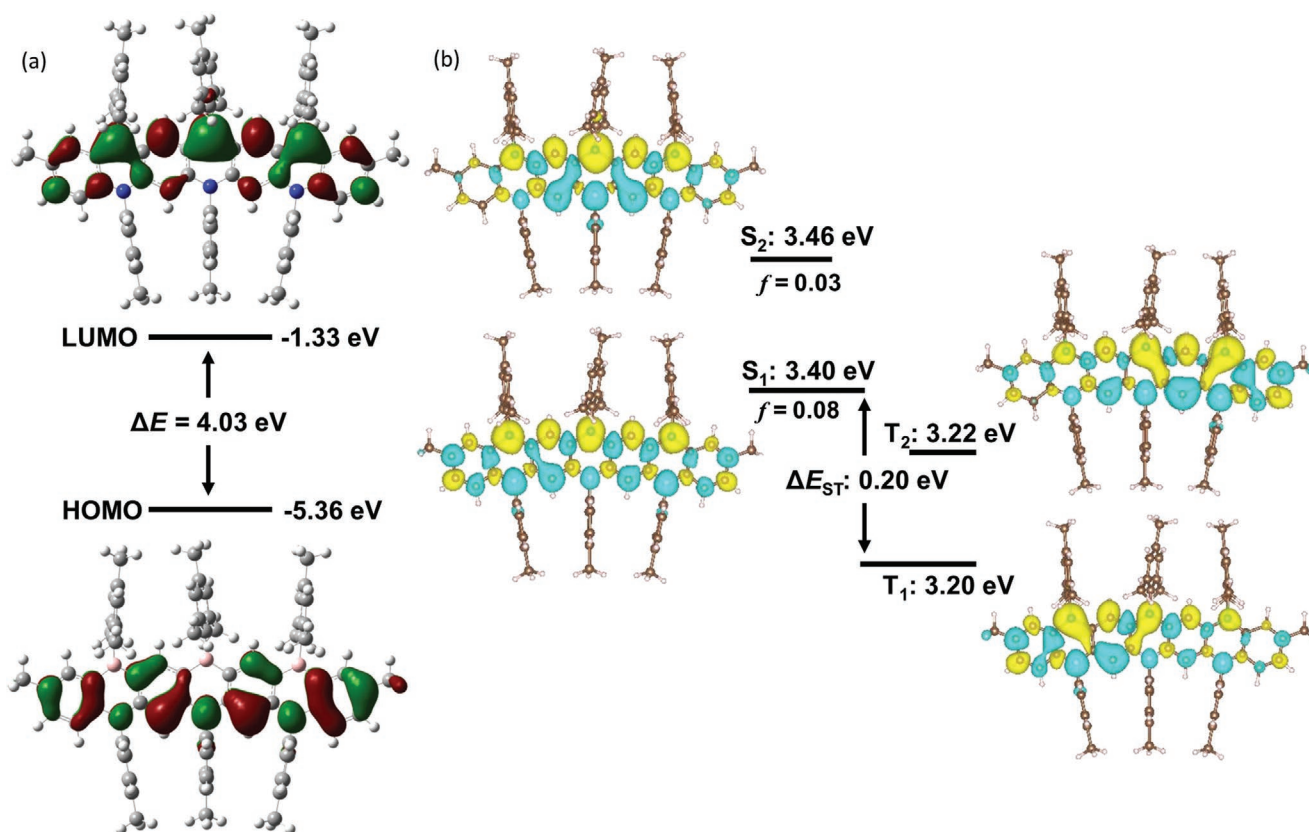
Figure 3. a) HOMO (bottom) and LUMO (top) energy distribution in *α*-3BNMes calculated using PBE0/6-31G (d,p), isovalue = 0.02; b) Difference density plots for the lowest-lying two singlets and triplets excited states for *α*-3BNMes calculated in the gas phase by using SCS-CC2/cc-pVDZ. Blue color represents an area of decreased electron density and yellow represents an increased electron density between the ground and excited states, isovalue = 0.001.

α-3BNOH, in *α*-3BNMes the heptacene core remains planar, and the aryl substituents attached to boron and nitrogen align nearly orthogonal to main acene core.

Computational modeling provides a clear description of this MR-TADF compound. DFT calculations at the PBE0/6-31G(d,p) level of theory in the gas phase predict a large HOMO-LUMO gap of 4.03 eV. The electron density distribution patterns of these orbitals is typical for MR-TADF compounds (**Figure 3**).[14] The HOMO density is mainly localized on the nitrogen and carbon atoms positioned *ortho* to them, while in the LUMO, electron density is mainly localized on the boron atoms and the carbons *ortho* to them. We applied spin component scaling second-order approximate coupled-cluster (SCS-CC2) to accurately predict the nature and energies of the excited states and the ΔE_{ST} (Figure 3b; Table S1, Supporting Information).[14,20,34] *α*-3BNMes shows a gratifyingly smaller ΔE_{ST} of 0.20 eV compared to that of *α*-3BNOH (ΔE_{ST} of 0.29 eV), but at the expense of a slightly smaller oscillator strength (*f*) for the transition to S$_1$ of 0.08 compared to *α*-3BNOH (*f* of 0.09).[32] The predicted S$_1$ energy is also stabilized to 3.40 eV compared to 3.69 eV in *α*-3BNMes. The difference density plot of the S$_1$ state shows the characteristic alternating pattern of increasing and decreasing electron density on adjacent atoms that is characteristic of MR-TADF compounds.[34] The patterns revealed in the difference density plots for T$_1$ and T$_2$ differ slightly from that of S$_1$. This

difference in the nature of the excited singlet and triplet states will result in enhanced spin-orbit coupling and assist in RISC following El Sayed's rules.[35]

The absorption spectrum was simulated by capturing transitions to the first five singlet excited states at the SCS-CC2/cc-pVDZ level of theory using DFT calculated ground state. Good agreement between the measured and simulated spectral shapes was obtained (Figure S9, Supporting Information). Similar trends in the difference density pictures of the lowest-lying singlet excitations were obtained for *α*-3BNMes (Figure S10, Supporting Information) compared to those of *α*-3BNOH,[32] explaining the near-identical shapes of their absorption spectra (**Figure 4**).

2.2. Optical Properties

Steady-state photophysical properties of both *α*-3BNMes and the previous *α*-3BNOH in dilute THF are shown in Figure 4. In the case of *α*-3BNMes, a bathochromic shift of 330 meV compared to *α*-3BNOH is observed in both the main *π*–*π** absorption band at 3.50 eV (354 nm) and the quasi degenerate S$_1$, S$_2$ SRCT excited states at 2.94 eV (421 nm). By replacing the strongly mesomerically electron-donating hydroxyl groups with inductively electron-withdrawing mesityl substituents, both the HOMO and LUMO levels are stabilized although the LUMO
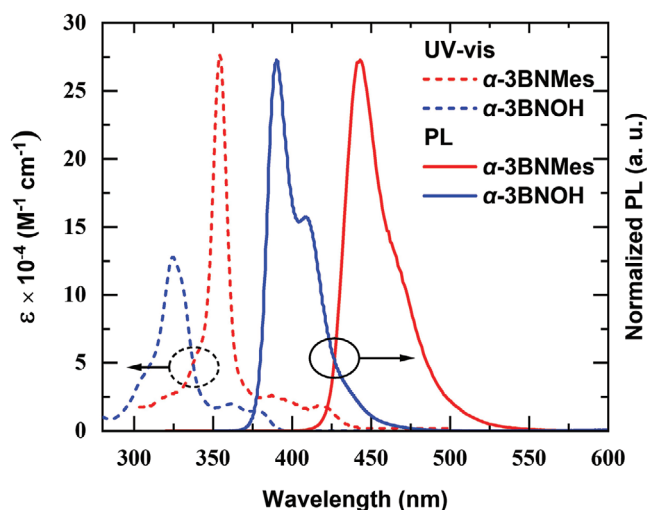
**ADVANCED
SCIENCE NEWS**

www.advancedsciencenews.com

**ADVANCED
OPTICAL
MATERIALS**

www.advopticalmat.de

Figure 4. Absorption (dotted line) and emission spectra (solid line) of *α*-**3BNMes** and *α*-**3BNOH** in dilute THF solution. λ_{exc} = 310 nm for emission spectra.

to a greater extent. This results in a net stabilization of the excited states in *α*-**3BNMes**, and red-shifts both its absorption and emission spectra. The molar extinction coefficient for the dominant high-energy band (S_4) is also increased by a factor of

two, although this still appears at very short wavelengths, and thus is unsuitable for FRET and HF OLED applications using available D–A TADF assistant dopants. Nonetheless, this demonstrates that significant control over the absorption spectrum is indeed possible. Promisingly, the HF device-relevant SRCT absorption bands at longer wavelengths are increased by a factor of 1.4 along with a useful red-shift to wavelengths beyond 400 nm in *α*-**3BNMes**.

Although these device-relevant SRCT bands remain smaller and at higher energies than in v-**DABNA** (Figure S11 Supporting Information, limiting HF compatibility with available D–A TADF cohosts), they still represent a significant improvement compared to *α*-**3BNOH**. It remains unclear how the structure of v-**DABNA** leads to its lowest-energy absorbance band becoming dominant, compared to the S_4 band in the heptacene systems. Computational and experimental work to further map out the largely unknown chemical space of MR-TADF emitters continues at pace both in our research groups and around the world.[29,36,37]

The solution photoluminescence spectrum of *α*-**3BNMes** shows a narrow emission centered at λ_{PL} = 2.80 eV (442 nm), with FWHM of 190 meV (30 nm) and a small Stokes shift of 140 meV (20 nm). Gratifyingly, the replacement of the hydroxyl groups with the mesityl substituents leads to a yet narrower, deep-blue emission, shifting the CIE coordinates of the PL spectrum from (0.17, 0.01) to (0.15, 0.04). These CIE 1931 values
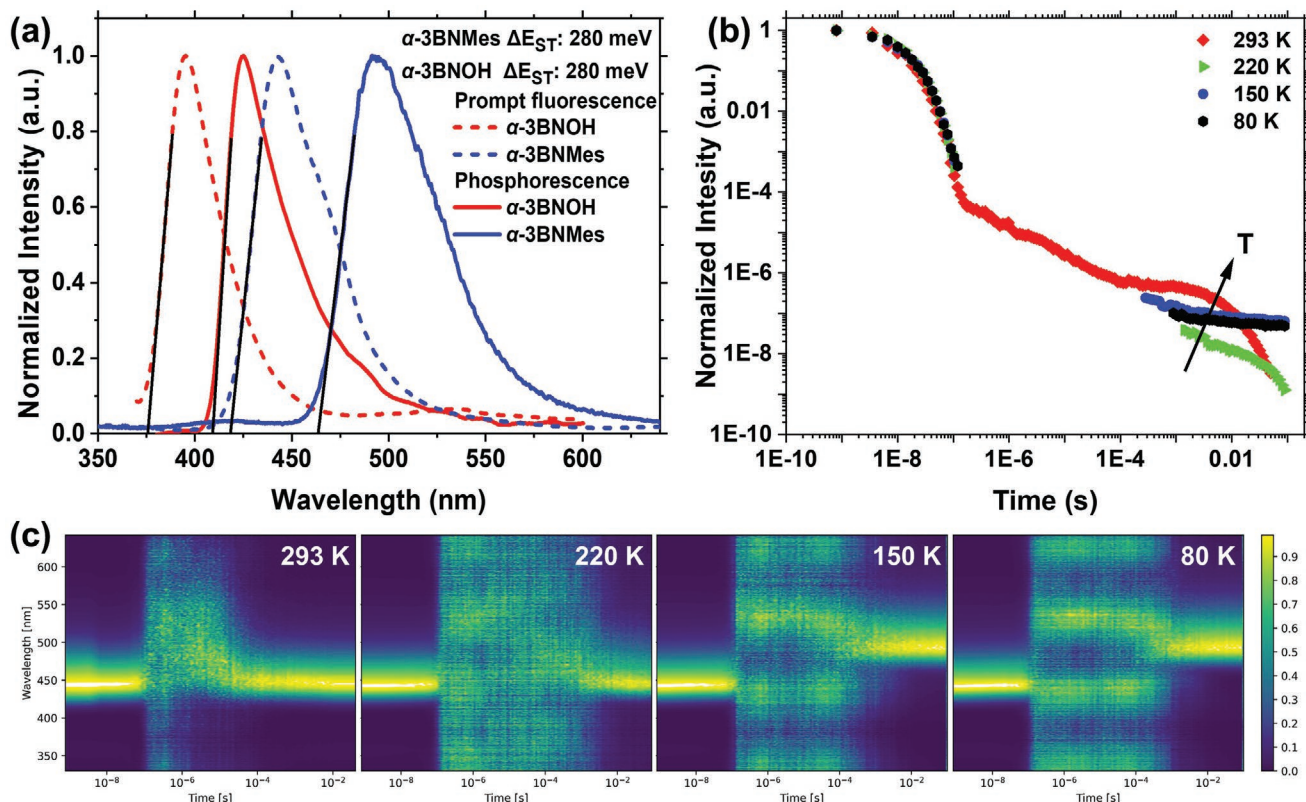

Figure 5. a) Time-resolved prompt fluorescence (prompt, delay time 10 ns and gate width 5 ns) and phosphorescence (delayed, delay time 70 ms and gate width 15 ms at 80 K) spectra of *α*-**3BNOH**[32] and *α*-**3BNMes** 1 wt% in PMMA. b) Temperature-dependent time-resolved emission decay of *α*-**3BNMes** 1 wt% in PMMA. c) Contour plots of time-resolved emission spectra at various temperatures (regions between 100 ns and 100 μs at lower temperatures represent background collection, i.e., no emission). λ_{exc} = 355 nm.

2200688 (5 of 9)

are considered ideal for blue OLEDs as defined by BT.2020-2.[1] Together, these THF solution results establish the absorption- and emission-tuning abilities of the boron substituents toward synthetic control of the singlet states of the B,N-heptacene core.

The solid-state fluorescence and phosphorescence spectra are shown in **Figure 5**a. As we have already established the red-shifting behavior of the singlet states in identical THF environments, this allows us to consider the trends of the energies of the triplet states (from film phosphorescence) more broadly. We find that the ΔE_{ST} are very similar in both materials, indicating that mesityl substitution of the boron atoms results in similar changes to both the singlet and triplet state energies of **α-3BNMes** compared to **α-3BNOH**.

Time-resolved photoluminescence decays of **α-3BNMes** doped at 1 wt% in PMMA matrix are shown in Figure 5b. Similar to previous reports of the photophysics of **α-3BNOH**[32] and many other reported MR-TADF materials, the delayed fluorescence from **α-3BNMes** is weak and long-lived compared to D–A TADF materials,[8,9,38,39] indicating only a moderate rate of rISC. When measured at lower temperatures, the delayed emission component (after 100 ns) is suppressed, evidencing the thermally activated mechanism of this emission. At longer delay times (beyond 0.1 ms) and at temperatures below 150 K the emission decay rate changes significantly, which along with a strong spectral red-shift identifies the phosphorescence regime from which the phosphorescence spectrum (Figures 5a,c) is extracted.

Exponential fitting of the room temperature decay reveals three different components: the prompt fluorescence has a lifetime, τ_p, of 10 ns, and there are two main components to the delayed emission with lifetimes of 9.08 µs and 7.06 ms (Figure S12a, Supporting Information). The shorter of the delayed lifetimes, corresponding to a regime of dual emission, is attributed to simultaneous emission from a monomer and a red-shifted aggregate species (Figures 5c; Figure S12c, Supporting Information), most probably associated with excimer emission as described by Stavrou et al.,[16] which is common in planar MR-TADF emitters. Notably, the contribution to the emission decay from this species is minimal and energetically is at the same positions as for **α-3BNOH**.[32] The longest delayed component is attributed to pure monomer emission with mono-excitonic origin as demonstrated in the power dependence measurement, in Figure S13 (Supporting Information). In contrast, **α-3BNOH** was found to have bi-excitonic TTA contribution, but we do not observe any quadratic-to-linear (slope 2 to slope 1) regime change in the DF intensity as excitation pulse energy is increased for **α-3BNMes**.[32]

As in other recent studies of MR-TADF materials,[16,19] and in strong contrast to the CT states of D–A TADFs,[7,9] we find that changing the host matrix has only the modest influence on the SRCT states and their TADF properties (Figure S12b, Supporting Information). The photoluminescence quantum yield (PLQY) of **α-3BNMes** in 1% mCP doped film was determined to be 63%, thus nearly double that of **α-3BNOH** (35% in 1 wt% mCP), and also sufficiently high to support OLED applications. Finally, using the determined PLQY, along with the time-resolved PL decay lifetimes the fluorescence (k_f), intersystem crossing (k_{ISC}), and reverse intersystem crossing (k_{RISC}) rate constants in mCP were estimated, according to Wada et al.[40] These were found to be 5.25×10^7 s^{-1} for k_f, 1.98×10^7 s^{-1} for k_{ISC} and 5.9×10^2 s^{-1}

for k_{RISC}. These values represent a fast k_f (as expected for a rigid polycyclic aromatic hydrocarbon), a reasonably fast rate of ISC (enabled by the SRCT states of the B,N network), and a low rate of RISC, which is still common amongst MR-TADF emitters due to their upper-state T_n-S_1 RISC mechanism.[16]

2.3. Devices

Having confirmed the weak TADF activity of **α-3BNMes**, its use as an emitter in OLEDs was nonetheless preliminarily assessed. Devices using a stack of ITO (anode) | NPB (HIL/HTL, 40 nm) | mCBP (EBL, 10 nm) | **α-3BNMes**:host X% (EML, 30 nm) | T2T (HBL, 10 nm) | T2T:LiQ 45% (EIL/ETL, 35 nm) | Al (cathode, 100 nm) were fabricated, with representative performance shown in Figure S14 (Supporting Information). Two different hosts were used, DPEPO (electron transporting, E_T = 3.05 eV) and mCBP (hole transporting and otherwise similar to mCP, and with E_T = 2.85 eV now confirmed high enough to be compatible with the emitter E_T = 2.7 eV), with varying concentrations of **α-3BNMes** ranging from 5 up to 20 vol%. With increasing doping concentration, no significant differences were observed in the current density–voltage–luminance (jVL) curves, the spectra, or EQE as a function of current density in both host environments. Consequently, we do not anticipate qualitatively different behavior in MR-TADF only devices with lower doping concentration, which were not investigated. More interestingly, no broadening of the electroluminescence (EL) spectrum was observed upon increasing concentration, indicating suppression of excimer formation even at high concentrations, a very common phenomenon of other MR-TADF emitters in films. Maximum EQEs of 1.7% at ≈100 cd m^{-2} were achieved in devices with each of the two hosts. We suggest that this poor performance is due to the weak TADF (slow k_{RISC}) of the material, leading to low efficiency combined with additional efficiency roll-off from the known instability of DPEPO,[12,41] especially at high current densities (Figure S14c, Supporting Information). Nonetheless, the CIE coordinates are very attractive at (0.15 and 0.08), which are the same as in the photo-excited film and similar to that determined in THF solution.

To compensate for the poor intrinsic exciton harvesting performance of **α-3BNMes** while still taking advantage of its ideal emission spectrum, we then applied it as a terminal emitter in HF OLEDs in combination with a D–A(-D) TADF sensitizer. In order to ensure adequate spectral overlap necessary for the energy transfer, we employed 2,8-bis(2,7-di(*tert*-butyl)-9,9-dimethylacridin-10(9*H*)-yl)dibenzo[b,d]thiophene (**DtBuAc-DBT**) as a TADF cohost, previously reported to give ~11% EQE$_{max}$ with CIE coordinates of (0.16, 0.17), and suitably high-energy blue emission to overlap with the absorption spectrum of **α-3BNMes**.[8] This D–A-D TADF assistant dopant was co-evaporated at 25 vol% in the EML, alongside 1 vol% **α-3BNMes** and 74 vol% DPEPO. The device architecture was chosen to be the same as the one previously reported,[8] with the addition of **α-3MesBN** as the terminal emitter, using ITO (anode)| NPB (HTL, 40 nm) | TSBPA (EBL, 10 nm) | **α-3BNMes**:DtBuAc-DBT:DPEPO 1:25:74% (EML, 30 nm) | DPEPO (HBL, 10 nm) | TBPi (ETL, 40 nm) | LiF (EIL, 1 nm) | Al (cathode, 100 nm). Both control "D–A-D only" (TADF) and combined HF OLED
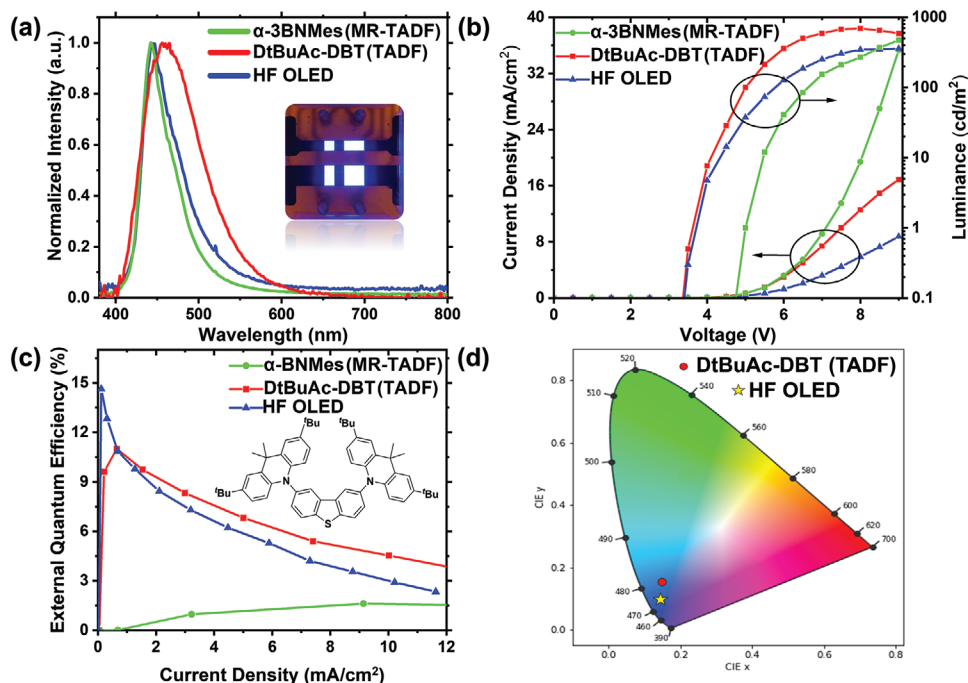
Figure 6. Performance of MR-TADF (green), D–A–D (red), and HF (blue) OLEDs. a) EL spectra. Inset: Operating HF OLED. b) jVL characteristics. c) EQE versus Current density. Inset: **DtBuAc-DBT** structure. d) CIE coordinates.

devices were produced in the same deposition run to provide a suitable comparison.

The resulting HF OLEDs possess good efficiency, with an EQE_{max} of 15% and an EQE_{100} (at 100 cd m^{-2}) of 10.2%, with a FWHM of 290 meV (49 nm) and CIE of (0.15 and 0.10), which is enabled by triplet harvesting by the D–A–D sensitizer, together with narrow deep blue emission from the **α-3BNMes** (**Figure 6**). Although the EQE_{max} is improved at 15% in the HF OLED (compared to 11% for the **DtBuAc-DBT** device) the larger roll-off at higher current densities results to an EQE_{300} of 6.2% and 8.8% for the HF and TADF OLEDs, respectively. Some of this roll-off is undoubtedly due to the known instability of the DPEPO host, the use of which is made necessary due to the requirements of the D–A TADF assistant dopant. This host instability frequently leads to DPEPO-based TADF OLEDs having poor device lifetimes, unsuitable for practical applications.[12,41] The OLEDs here also suffer from poor stability for these reasons, and so their operational lifetimes were not directly assessed. However, the strategy of expanding HF compatibility through red-shifted absorption may in the future allow blue HF OLEDs to use red-shifted D–A TADF cohosts and lower-E_T bulk hosts with improved stability.

The differences in EQE at different driving regimes are a result of compromise between detrimental factors (e.g., the moderate PLQY of **α-3BNMes** as the terminal emitter, competing unproductive Dexter energy transfer, in-situ charge trapping, etc.) and beneficial effects (e.g., **α-3BNMes** alignment/anisotropic emission and good FRET overlap outcompeting **DtBuAc-DBT** non-radiative decay), although some of these factors are deceptively difficult to quantify by established experimental methods.[27] The overall HF OLED performance

is nonetheless competitive with other recent leading reports at similar color coordinates (Figure S16 and Table S2, Supporting Information).

The EL spectrum of the HF OLEDs is nearly identical to the **α-3BNMes** spectrum, indicating efficient FRET with only a small contribution of the D–A–D TADF sensitizer at ~525 nm. This efficient FRET is in good agreement with the calculated FRET radius of 2.27 nm, using the spectral overlap in Figure S15 (Supporting Information) and classical energy transfer models.[16] This result in particular highlights the importance and challenge of both emission and absorption spectral tuning for developing high-efficiency blue HF OLED material combinations. While it is incredibly challenging to further deepen the emission color of available D–A-D TADF assistant dopants, the need to do so can be avoided in HF OLEDs by instead red-shifting the absorption spectrum of the MR-TADF terminal emitters, as we demonstrate here. Similarly, while stable high-triplet hosts with good charge transport properties remain elusive, the need for these could be circumvented in future if FRET compatibility for MR-TADFs can be extended to cyan of green D–A TADFs, for which suitable hosts are much more attainable.

3. Conclusions

We have achieved emission and absorption color tuning in a deep blue non-triangulene type MR-TADF compound by altering the boron substituents in a B, N-doped heptacene. Compared to the parent UV emitter **α-3BNOH**, these changes imbue **α-3BNMes** with ideal CIE coordinates for blue OLEDs and suitable absorption spectrum for FRET

compatibility with existing D–A TADF cohosts. The resulting HF OLEDs achieved an EQE_{max} of 15% and deep-blue color coordinates of (0.15 and 0.10), compared to <1% efficiencies for the unassisted α-**3BNOH**. In light of slow progress toward the development of truly deep-blue D–A TADF emitters (and their accompanying hosts), we advance that controlling the absorption spectrum of terminal MR-TADF emitters to expand FRET compatibility in HF devices is a more fruitful approach.

Supporting Information

Supporting Information is available from the Wiley Online Library or from the author.

Conflict of Interest

The authors declare no conflict of interest.

Data Availability Statement

The research data supporting this publication are openly available on the Research portal of the University of St Andrews at https://doi.org/10.17630/8978d1ac-35f4-4f16-932a-c0d1d32f6317.

[1] International Telecommunication Union (ITU), Recommendation ITU-R BT.2020-2, **2015**.
[2] R. Seidel, *SMPTE Motion Imaging J.* **2014**, *123*, 18.
[3] Y. Takita, K. Takeda, N. Hashimoto, S. Nomura, T. Suzuki, H. Nakashima, S. Uesaka, S. Seo, S. Yamazaki, *J. Soc. Inf. Disp.* **2018**, *26*, 55.
[4] N. Hashimoto, Y. Takita, R. Yamaoka, S. Nomura, T. Sasaki, S. Yamagata, T. Suzuki, S. Seo, *SID Symp. Dig. Tech. Pap.* **2017**, *48*, 786.
[5] M. Y. Wong, E. Zysman-Colman, *Adv. Mater.* **2017**, *29*, 1605444.
[6] R. Ansari, W. Shao, S.-J. Yoon, J. Kim, J. Kieffer, *ACS Appl. Mater. Interfaces* **2021**, *13*, 28529.
[7] K. Stavrou, L. G. Franca, A. P. Monkman, *ACS Appl. Electron. Mater.* **2020**, *2*, 2868.
[8] R. Huang, N. A. Kukhta, J. S. Ward, A. Danos, A. S. Batsanov, M. R. Bryce, F. B. Dias, *J. Mater. Chem. C* **2019**, *7*, 13224.
[9] P. Stachelek, J. S. Ward, P. L. dos Santos, A. Danos, M. Colella, N. Haase, S. J. Raynes, A. S. Batsanov, M. R. Bryce, A. P. Monkman, *ACS Appl. Mater. Interfaces* **2019**, *11*, 27125.
[10] P. L. dos Santos, D. Chen, P. Rajamalli, T. Matulaitis, D. B. Cordes, A. M. Z. Slawin, D. Jacquemin, E. Zysman-Colman, I. D. W. Samuel, *ACS Appl. Mater. Interfaces* **2019**, *11*, 45171.
[11] I. A. Wright, A. Danos, S. Montanaro, A. S. Batsanov, A. P. Monkman, M. R. Bryce, *Chem. – A Eur. J.* **2021**, *27*, 6545.
[12] S. Ihn, D. Jeong, E. S. Kwon, S. Kim, Y. S. Chung, M. Sim, J. Chwae, Y. Koishikawa, S. O. Jeon, J. S. Kim, J. Kim, S. Nam, I. Kim, S. Park, D. S. Kim, H. Choi, S. Kim, *Adv. Sci.* **2022**, *9*, 2102141.
[13] J. M. Ha, S. H. Hur, A. Pathak, J.-E. Jeong, H. Y. Woo, *NPG Asia Mater* **2021**, *13*, 53.
[14] S. M. Suresh, D. Hall, D. Beljonne, Y. Olivier, E. Zysman-Colman, *Adv. Funct. Mater.* **2020**, *30*, 1908677.
[15] A. Monkman, *ACS Appl. Mater. Interfaces* **2021**, *13*, 20463.
[16] K. Stavrou, A. Danos, T. Hama, T. Hatakeyama, A. Monkman, *ACS Appl. Mater. Interfaces* **2021**, *13*, 8643.
[17] T. Northey, T. J. Penfold, *Org. Electron.* **2018**, *59*, 45.
[18] I. Kim, K. H. Cho, S. O. Jeon, W.-J. Son, D. Kim, Y. M. Rhee, I. Jang, H. Choi, D. S. Kim, *JACS Au* **2021**, *1*, 987.
[19] D. Hall, K. Stavrou, E. Duda, A. Danos, S. Bagnich, S. Warriner, A. M. Z. Slawin, D. Beljonne, A. Köhler, A. Monkman, Y. Olivier, E. Zysman-Colman, *Mater. Horiz.* **2022**, *9*, 1068.
[20] A. Pershin, D. Hall, V. Lemaur, J.-C. Sancho-Garcia, L. Muccioli, E. Zysman-Colman, D. Beljonne, Y. Olivier, *Nat. Commun.* **2019**, *10*, 597.
[21] D. Hall, S. M. Suresh, P. L. dos Santos, E. Duda, S. Bagnich, A. Pershin, P. Rajamalli, D. B. Cordes, A. M. Z. Slawin, D. Beljonne, A. Köhler, I. D. W. Samuel, Y. Olivier, E. Zysman-Colman, *Adv. Opt. Mater.* **2020**, *8*, 1901627.
[22] E. Zysman-Colman, *Nat. Photonics* **2020**, *14*, 593.
[23] J. H. Kim, W. J. Chung, J. Kim, J. Y. Lee, *Mater. Today Energy* **2021**, *20*, 100792.
[24] S. O. Jeon, K. H. Lee, J. S. Kim, S.-G. Ihn, Y. S. Chung, J. W. Kim, H. Lee, S. Kim, H. Choi, J. Y. Lee, *Nat. Photonics* **2021**, *15*, 208.
[25] D. Zhang, X. Song, A. J. Gillett, B. H. Drummond, S. T. E. Jones, G. Li, H. He, M. Cai, D. Credgington, L. Duan, *Adv. Mater.* **2020**, *32*, 1908355.
[26] C.-Y. Chan, M. Tanaka, Y.-T. Lee, Y.-W. Wong, H. Nakanotani, T. Hatakeyama, C. Adachi, *Nat. Photonics* **2021**, *15*, 203.
[27] N. Haase, A. Danos, C. Pflumm, P. Stachelek, W. Brütting, A. P. Monkman, *Mater. Horiz.* **2021**, *8*, 1805.
[28] H. Nakanotani, T. Higuchi, T. Furukawa, K. Masui, K. Morimoto, M. Numata, H. Tanaka, Y. Sagara, T. Yasuda, C. Adachi, *Nat. Commun.* **2014**, *5*, 4016.
[29] H. Tanaka, S. Oda, G. Ricci, H. Gotoh, K. Tabata, R. Kawasumi, D. Beljonne, Y. Olivier, T. Hatakeyama, *Angew. Chem., Int. Ed.* **2021**, *60*, 17910.
[30] M. Yang, I. S. Park, T. Yasuda, *J. Am. Chem. Soc.* **2020**, *142*, 19468.

[31] J. Li, F. Zhao, Y. Chen, M. Zhang, T. Li, H. Zhang, *J. Mater. Chem. C* **2021**, *9*, 15309.

[32] S. M. Suresh, E. Duda, D. Hall, Z. Yao, S. Bagnich, A. M. Z. Slawin, H. Bässler, D. Beljonne, M. Buck, Y. Olivier, A. Köhler, E. Zysman-Colman, *J. Am. Chem. Soc.* **2020**, *142*, 6588.

[33] S. M. Suresh, E. Duda, F.-J. Kahle, D. Hall, S. Bagnich, H. Bässler, D. Beljonne, Y. Olivier, A. Köhler, E. Zysman-Colman, S. I. D. Symp, *Dig. Tech. Pap.* **2021**, *52*, 228.

[34] D. Hall, J. C. Sancho-Garcia, A. Pershin, D. Beljonne, E. Zysman-Colman, Y. Olivier, *ChemRxiv* **2021**, https://doi.org/10.33774/chemrxiv-2021-496gn.

[35] M. K. Etherington, J. Gibson, H. F. Higginbotham, T. J. Penfold, A. P. Monkman, *Nat. Commun.* **2016**, *7*, 13680.

[36] S. M. Pratik, V. Coropceanu, J. L. Brédas, *ACS Mater. Lett.* **2022**, *4*, 440.

[37] M. Nagata, H. Min, E. Watanabe, H. Fukumoto, Y. Mizuhata, N. Tokitoh, T. Agou, T. Yasuda, *Angew. Chem., Int. Ed.* **2021**, *60*, 20280.

[38] J. S. Ward, A. Danos, P. Stachelek, M. A. Fox, A. S. Batsanov, A. P. Monkman, M. R. Bryce, *Mater. Chem. Front.* **2020**, *4*, 3602.

[39] N. A. Kukhta, H. F. Higginbotham, T. Matulaitis, A. Danos, A. N. Bismillah, N. Haase, M. K. Etherington, D. S. Yufit, P. R. McGonigal, J. V. Gražulevičius, A. P. Monkman, *J. Mater. Chem. C* **2019**, *7*, 9184.

[40] Y. Wada, H. Nakagawa, S. Matsumoto, Y. Wakisaka, H. Kaji, *Nat. Photonics* **2020**, *14*, 643.

[41] S.-G. Ihn, N. Lee, S. O. Jeon, M. Sim, H. Kang, Y. Jung, D. H. Huh, Y. M. Son, S. Y. Lee, M. Numata, H. Miyazaki, R. Gómez-Bombarelli, J. Aguilera-Iparraguirre, T. Hirzel, A. Aspuru-Guzik, S. Kim, S. Lee, *Adv. Sci.* **2017**, *4*, 1600502.